

Selection biases in empirical $p(z)$ methods for weak lensing

D. Gruen^{1,2*} and F. Brimiouille³

¹SLAC National Accelerator Laboratory, Menlo Park, CA 94025, USA

²KIPAC, Physics Department, Stanford University, Stanford, CA 94305, USA

³Max Planck Institute for Extraterrestrial Physics, Giessenbachstrasse, 85748 Garching, Germany

ABSTRACT

To measure the mass of foreground objects with weak gravitational lensing, one needs to estimate the redshift distribution of lensed background sources. This is commonly done in an empirical fashion, i.e. with a reference sample of galaxies of known spectroscopic redshift, matched to the source population. In this work, we develop a simple decision tree framework that, under the ideal conditions of a large, purely magnitude-limited reference sample, allows an unbiased recovery of the source redshift probability density function $p(z)$, as a function of magnitude and colour. We use this framework to quantify biases in empirically estimated $p(z)$ caused by selection effects present in realistic reference and weak lensing source catalogues, namely (1) complex selection of reference objects by the targeting strategy and success rate of existing spectroscopic surveys and (2) selection of background sources by the success of object detection and shape measurement at low signal-to-noise. For intermediate-to-high redshift clusters, and for depths and filter combinations appropriate for ongoing lensing surveys, we find that (1) spectroscopic selection can cause biases above the 10 per cent level, which can be reduced to ≈ 5 per cent by optimal lensing weighting, while (2) selection effects in the shape catalogue bias mass estimates at or below the 2 per cent level. This illustrates the importance of *completeness* of the reference catalogues for empirical redshift estimation.

Key words: cosmology: observations – galaxies: distances and redshifts – gravitational lensing: weak

1 INTRODUCTION

Weak gravitational lensing enables measurements of the mass distribution of foreground structures in the Universe by the distortion that their tidal gravitational fields impose on the images of background galaxies. The amplitude of the weak lensing shear γ_t is proportional to both the surface mass density of the structure acting as the lens and the geometry of the observer-lens-source system,

$$\gamma_t \propto D_d \frac{D_{ds}}{D_s} =: D_d \beta, \quad (1)$$

where D_d , D_{ds} and D_s are the angular diameter distances from observer to lens, and from lens and observer to source, respectively (e.g. Bartelmann & Schneider 2001, their section 3.1.2), and we have defined β as the ratio of the latter. In order to use lensing to constrain the properties of the lens and the expansion of the Universe, one therefore needs to know the redshifts of lensed sources or – sufficiently, because

weak lensing is only ever measured on ensembles of sources – their redshift distribution.

Knowledge of true source redshifts, e.g. from spectroscopic follow-up of each source galaxy, would allow for a lensing analysis that is both unbiased (because one could account for the geometry of lenses and sources exactly) and statistically optimally powerful (because one could select only true background sources and weight each source galaxy according to its expected signal in a minimum-variance estimator of mean shear). Unfortunately, however, complete, spectroscopic follow-up of large samples of faint galaxies is not feasible with present technology. One therefore has to resort to approximate methods based on photometric properties of the source galaxy population.

When high quality photometric information is available, redshifts of source galaxies can be determined from fitting redshifted template galaxy spectral energy distributions (SEDs) to the photometric flux measurements (e.g. Loh & Spillar 1986; Arnouts et al. 1999; Benítez 2000; Bender et al. 2001; Ilbert et al. 2006; Brammer et al. 2008). In the limit of photometric coverage over a wide range of wavelength and with a large number of narrow-band fil-

* Einstein Fellow; e-mail: dgruen@stanford.edu

ters, the resulting template fitting photometric redshifts can be determined almost unambiguously for each galaxy, i.e. with small statistical uncertainties, little ambiguity between different combinations of galaxy type and redshift, and almost full completeness. For less optimal photometric data, e.g. when photometry is available only in a smaller range of bands, degeneracies between redshift and galaxy type for a given set of observed fluxes allow only for a probabilistic description of the redshift of each source, which crucially depends on assumed priors regarding the prevalence of galaxy types as a function of redshift and luminosity. This is the case particularly for ongoing and upcoming four-to-six-band surveys like the Dark Energy Survey (DES, Jarvis et al. 2016), the Kilo Degree Survey (KiDS, Kuijken et al. 2015), the Hyper-Suprime Cam Survey (HSC, <http://hsc.mtk.nao.ac.jp/ssp/>), and LSST (LSST Science Collaboration et al. 2009).

An alternative approach, which we will refer to as *empirical*, is to compare each source galaxy to a reference sample of galaxies with known (spectroscopic) redshift. The redshift z , or redshift distribution $p(z)$, assigned to the source galaxy is found from the redshifts of reference galaxies similar to it in terms of their photometric properties. Given a sufficiently large reference catalogue of galaxies selected in the same way as a photometric sample, the redshift distribution of the latter can be inferred from the redshift distribution of the former, both for individual sources and for the overall sample.

In practical application, a number of effects can lead to sub-optimal or biased results in empirical methods, e.g. because

- photometric information on source galaxies is noisy and/or available only in few bands. When galaxies of a range of redshifts have indistinguishable observed properties, selection of sources and weighting by the amplitude of their lensing signal are not possible in a statistically optimal way. For small reference catalogues or surveys, poor photometry also exacerbates cosmic variance.

- selection effects in the source catalogue are not applied to the reference sample. Because weak lensing measurements are often limited by noise due to the intrinsic shape of background galaxies, one typically uses source samples that extend beyond the magnitude limit where the catalogue is complete. In addition, shape measurement of galaxies has success rates significantly below unity, even for galaxies with highly significant photometric detections. Both of these selection effects depend on the size and other morphological properties of source galaxies. If, at a given position in colour-magnitude space, these properties correlate with redshift, biases are introduced.

- selection effects are present in the reference catalogue that do not apply to the source sample. Most spectroscopic surveys have selected targets by a combination of colours, magnitude and sometimes additional morphological properties. Biases are introduced when some of these do influence the redshift distribution but are not taken into account when estimating $p(z)$, e.g. because they are not measured for the source galaxies. However, even when the target selection is applied to the source galaxy sample, the incompleteness of spectroscopic surveys and the fact that, especially at the faint end, success of spectroscopic redshift recovery de-

pends strongly on galaxy type and redshift (e.g. on whether prominent emission lines fall inside the accessible wavelength range of a spectrograph), can cause additional biases.

The expectation value of β for a lens redshift z_d is estimated from $p(z)$ as

$$\langle\beta\rangle(z_d) = \int \frac{D_{ds}(z, z_d)}{D_s(z)} p(z) dz. \quad (2)$$

Biases in $p(z)$ therefore result in biases in $\langle\beta\rangle$. For the purposes of lensing measurements of foreground structure, it is useful to describe systematic errors in an object's $p(z)$ by deviations of $\langle\beta\rangle$ from its true mean for a sample of source galaxies.

In this work, we quantify these systematic effects on empirical $p(z)$ estimation. To this end, we develop a simple colour-magnitude decision tree in section 2, based on a magnitude limited reference sample with spectroscopically calibrated photometric redshifts from CFHTLS Deep optical and WIRDS near-infrared photometry. In section 3, we measure the effect of selection biases in spectroscopic subsamples, and due to the success of object detection and shape measurement in noisy data. We conclude in section 4. We describe three straightforward applications of the methodology presented in this paper to quantify the statistical power (Appendix A) and cosmic variance (Appendix B) of empirical photometric redshifts as a function of bands used, and estimate biases in photometric redshifts from lensing magnification in Appendix C.

All magnitudes used in this work are defined in the AB system and for CFHT Megacam / WIRCam filters u^* (u.MP9301), g' (g.MP9401), r' (r.MP9601), i' (i.MP9701), i'_2 (i.MP9702, denoted y elsewhere), z' (z.MP9801), J (J.WC8101), H (H.WC8201) and K_s (Ks.WC8302). Cosmological distances for the scaling of lensing signal amplitudes are calculated in a flat Λ cold dark matter cosmology with $\Omega_m = 0.27$.

2 METHOD

Photometric redshift methods aim to characterize the probability density function (PDF) of the redshift of a galaxy, $p(z)$, or more specifically the conditional PDF w.r.t. its observed photometric properties. A useful frequentist understanding of the conditional $p(z)$ is that it is the distribution of true redshifts one would find in a complete spectroscopic follow-up of a large number of galaxies that look similar to the one in question in terms of its photometric properties.

Empirical redshift methods estimate a galaxy's $p(z)$ from the distribution of known true redshifts of similar galaxies. *Similar* in this case refers to the observed properties of the galaxy in question, e.g. magnitudes in the filter bands of some survey. Methods differ by how they establish similarity, e.g. by interpolation of a (complicated) functional form such as for the case of artificial neural networks, kernel averaging in the space of observed parameters, or classification into subsamples. The optimal use of reference catalogues for redshift estimation has been explored with various statistical and machine learning techniques (e.g. Connolly et al. 1995; Firth et al. 2003; Collister & Lahav 2004; Lima et al. 2008; Carrasco Kind & Brunner 2013;

Sadeh et al. 2016; Hoyle et al. 2015; Rau et al. 2015; Hoyle 2016).

In the following sections, we describe the framework used in this work to test selection effects in empirical redshift estimation with a simple colour-magnitude decision tree applied to a magnitude-limited reference sample of galaxies with high-quality photometric redshift estimates.

2.1 Construction of colour-magnitude decision tree

As a framework for investigating systematic effects of empirical redshift methods, we develop a simple scheme based on classification of a magnitude-limited reference sample of galaxies using a decision tree in colour-magnitude space. By taking care to treat statistical limits of photometric measurements of colours correctly, our scheme yields unbiased estimates of $p(z)$ in the absence of selection effects.

The purpose of the scheme is to describe the dependence of redshift on colour and magnitude adequately, yet with minimal complexity and in a way that allows systematic studies of errors in $p(z)$ estimation.

To this end, for colour-magnitude information (c_1, \dots, c_n, m) , we define a set of boxes (i.e., hyper-rectangles) B_i in $(n + 1)$ -dimensional space as

$$B_i =]c_{1,i}^{\min}, c_{1,i}^{\max}] \times \dots \times]c_{n,i}^{\min}, c_{n,i}^{\max}] \times]m_i^{\min}, m_i^{\max}]. \quad (3)$$

Each source that falls into B_i is assigned the observed distribution of redshifts of reference galaxies in B_i as its $p(z)$.

To build the decision tree from a reference catalogue of galaxies with known redshift (and, therefore, β for a given lens redshift z_d), we

- (i) split the sample into two equally sized subsamples 1 and 2 at the median of each of the $n + 1$ properties, then
- (ii) select the property where the split yields the maximal value of $\langle \beta \rangle_1^2 + \langle \beta \rangle_2^2$, and finally
- (iii) accept the split unless a stopping criterion is fulfilled and continue to both subsamples further.

The condition (ii) for the optimal split can be understood from considering the recovered lensing signal-to-noise ratio (S/N) from the optimally weighted source sample (cf. Appendix A).

A split is performed only if all of the following criteria are met:

- the split is such that for all of the galaxies in the reference subsample, all of the relevant bands defining the new subsamples are measured with a S/N of flux of at least 10,
- the difference between $\langle \beta \rangle_1$ and $\langle \beta \rangle_2$ is larger than twice its uncertainty estimated from the sample variance in the subsample, and
- the subsamples contain at least 100 reference galaxies.

Once, for a subsample, splits at the median of none of the properties meet these criteria, we stop and use its limits as a colour-magnitude box. Figure 1 illustrates the tree structure in 2D generated from $i', r' - i'$ information for a lens redshift of $z_d = 0.5$.

We note that, while simplistic, the colour-magnitude decision tree employed in this work yields a self-consistent $p(z)$ estimate: applied to the reference sample itself (or a representative subsample thereof), the estimated $p(z)$ or β

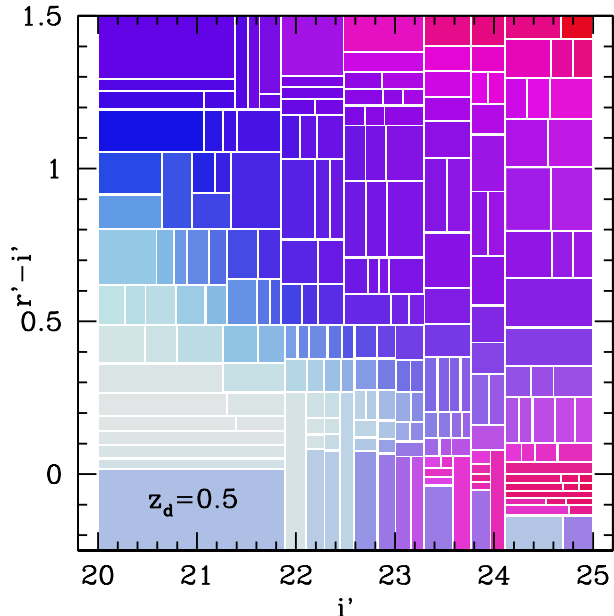


Figure 1. Decision tree for estimation of β at $z_d = 0.5$ from $i', r' - i'$ colour-magnitude information of source galaxies with $20 < i' < 25$. The colour of each box indicates the mean value of β (from 0, cyan, to the maximum, red) and the saturation of the level of recovery of lensing S/N relative to selection and weighting by spectroscopic redshifts (cf. Appendix A).

has the exact (expectation) value. And given a magnitude-limited catalogue of a certain depth and set of observed bands, it allows us to build appropriate decision trees for any shallower magnitude-limited sample observed in a subset of the bands. This is a potential advantage over simple kernel density estimation (where non-linear dependence of mean redshift on photometry over the range of the kernel causes a bias) or machine learning schemes. While it is conceivable that more elaborate methods yield smaller statistical uncertainties, i.e. in terms of the width of the $p(z)$ of individual galaxies, the decision tree method is a useful baseline for an empirical method that is unbiased when applied to reference catalogues and source samples in the absence of selection effects.

One limitation of the method is the effect of noise in the photometry of source galaxies for which the $p(z)$ should be estimated. With noisy flux measurements, measured and true magnitudes of galaxies can correspond to different colour-magnitude boxes. This is fully accounted for when galaxies in the reference catalogue and galaxies in the sample to which the method is applied are scattered between their true colour-magnitude box and surrounding boxes with the same probability. One way of achieving this would be to re-shuffle the reference galaxies between boxes according to noise added to their flux measurements to match the higher flux errors of the respective source galaxy. For all tests run in this work, however, we use the reference sample itself as source galaxies with the exact same flux measurements for building the tree, estimating the $p(z)$ of each cell, and assigning sources to cells, and such a procedure is therefore not necessary.

We note that estimating the $p(z)$ of a (sub)sample of

the galaxies used to build and populate the tree is advantageous for estimating the impact of selection effects, as in subsection 3.1, 3.2, and 3.3, or shifts in photometry, as in Appendix C, since it nulls the effect of sample variance. For evaluating the quality of the tree method for photometric redshift estimation, it would be preferable to use separate (*training* and *validation*) samples for populating the tree and finding the redshift distributions of. Given the large number of reference galaxies, we expect that our use of the full sample for both has only a minor impact on the results of Appendix A and Appendix B.

2.2 Reference catalogue

The empirical method developed and tests performed in this work rely on a reference sample of galaxies with known (true) redshifts and colour-magnitude information in a subset of the bands available for the galaxies we would like to estimate the $p(z)$ for. The reference catalogue needs to select galaxies only by their (extinction-corrected) total magnitude in a single band, i.e. should make no selection based on colour, size, type or observing conditions. Since no large and deep enough sample with spectroscopic redshifts is available that matches these criteria, we resort to a sample with high-quality photometric redshifts. The underlying assumption of the tests to follow is that these are the *true* redshifts of the reference sample of galaxies. The tests are defined, however, to be almost independent in their result from the validity of this assumption.

For the purpose of getting a useful sample of galaxies, we use imaging data in $u^*g'r'i'_2z'$ from the Canada-France-Hawaii Telescope Legacy Survey (CFHTLS) Deep fields,¹ overlapping with JHK_s data from the WIRCam Deep Survey (WIRDS, Bielby et al. 2012).

The catalogue creation follows the procedure described in Brimiouille et al. (2013). We use the SEXTRACTOR software (Bertin & Arnouts 1996) in dual-image mode to extract the photometric fluxes, magnitudes and errors. In order to obtain meaningful colour estimates, we at first adjust the PSF in the different observed filters by degradation to the value of the worst band (which is in general u^*). We do so by convolving the co-added images with an appropriate global Gaussian kernel so that the measured stellar colours in average no longer depend on the considered aperture. We then use the unconvolved i' -band as the detection band and extract the photometric fluxes from the convolved images, making use of weight images. We extract all objects that are at least 2σ above the background on at least four contiguous pixels. Unfortunately, the image zeropoints provided with CFHTLS Deep are of limited accuracy, which leads to field-to-field variations of colour. We account for this by applying a stellar locus regression, making use of the predicted stellar colours of the Pickles star library (1998), thus homogenizing the colour estimates in the different pointings. In the next step we obtain preliminary photometric redshift estimates using the template-fitting Photo-Z code of Bender et al. (2001), which has been successfully applied in a variety of lensing-related contexts (e.g. Brimiouille et al.

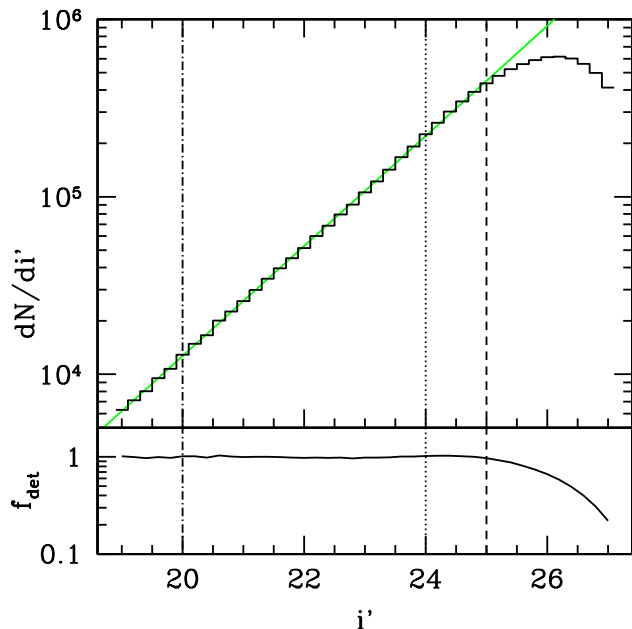


Figure 2. Upper panel: Distribution of apparent i' band magnitude of galaxies detected in the CFHTLS Deep fields. Green line indicates a power-law fit in the range $19 < i' < 22$. Lower panel: Completeness of object detection estimated relative to the power-law fit. Vertical lines indicate cuts for deep ($20 < i' < 25$) and shallow samples ($20 < i' < 24$) used later.

2013, Spinelli et al. 2012). In the final steps we then verify the achieved photometric redshift accuracy by comparison with the available spectroscopic overlap (see section 2.2.1) and use the information to apply the final spectroscopic calibration to our photometric redshift sample, obtaining a very good photometric redshift accuracy of $\sigma_{\Delta z/(1+z_{\text{spec}})} = 0.026$ and $\Delta z/(1+z) = 0.031$ in scatter and outlier rate of $\eta = 2.1$ per cent for galaxies with $i' \leq 24.0$ (cf. Figure 4).

Combining all CFHTLS Deep fields, this yields over one million galaxies detected down to $i \approx 27.5$. In order to ensure completeness, we however apply the following cuts.

We exclude objects above a level of background noise in any of the bands such that our sample has a signal-to-background-noise ratio of at least 10 in apertures of 8 pix (1.5 arcsec) diameter for $u^*, g', r' < 26.5$, $i' < 26$, $i'_2, z' < 25.5$. Infrared coverage is less uniform, such that while we require that objects are not masked in the WIRDS data, we include all area above limiting magnitudes of $J < 20$, $H < 19.5$ and $K_s < 19$. We ensure that for objects fainter than these magnitude limits, only an upper limit in flux at this magnitude is used for $p(z)$ estimation. We do *not*, however, reject objects with fluxes below these limits (i.e. drop-outs).

The only cut dependent on galaxy properties is that we exclude objects brighter than $i' = 20$, where $dN/di' < 5000$, or fainter than $i' = 25$, where dN/di' begins to deviate from a power-law (cf. Figure 2). A small number of objects (54 in total) need to be excluded from the sample because the template fit fails. This combination of cuts yields 348,601 galaxies in the four CFHT pointings (cf. Table 1). The redshift distribution of the deep and bright sample are shown in Figure Figure 3.

¹ <http://www.cfht.hawaii.edu/Science/CFHLS/cfhtlsdeepwidefields.html>

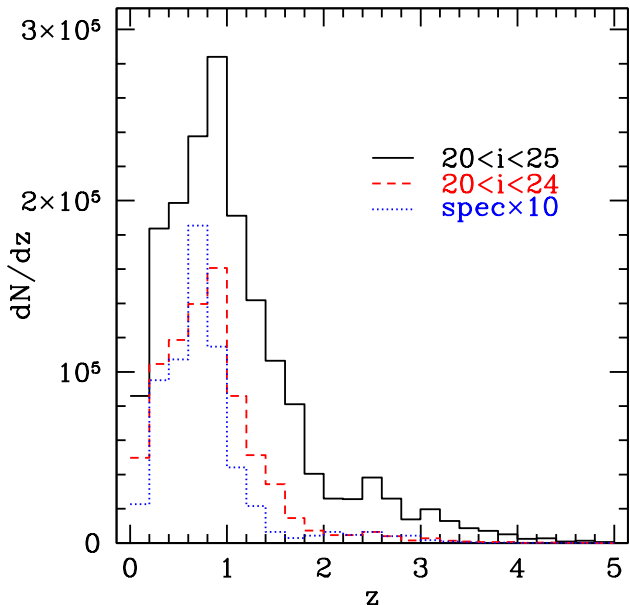


Figure 3. Distributions of template-fitting redshift point estimate for deep $20 < i' < 25$ sample (black, solid line), bright $20 < i' < 24$ sample (red, dashed line) and spectroscopic subsample (blue, dotted line, multiplied by 10 to match scale).

We note that the deep sample of $i' < 25$ is complete over the magnitude range of shape catalogues used for the CFHT Lensing Survey (CFHTLenS, Heymans et al. 2012; Miller et al. 2013) as well as the Weighing the Giants (WtG, von der Linden et al. 2014; Applegate et al. 2014) and COntstrain Dark Energy with X-ray clusters (CODEX, Cibirka et al. 2016) dedicated cluster weak lensing surveys. We define a bright subsample as $20 < i' < 24$, more representative of shape catalogues in ongoing large-area surveys such as DES (Jarvis et al. 2016) or KiDS (Kuijken et al. 2015), consisting of 159,065 galaxies.

Other publicly available, deep, high-quality photometric redshift catalogues, such as those of the COSMOS field (Ilbert et al. 2006, 2009; Laigle et al. 2016), the ESO Deep Public Survey (ESO-DPS, Erben et al. 2005; Hildebrandt et al. 2006), or the ALHAMBRA survey (Molino et al. 2013) are less useful for the tests performed here due to a combination of smaller area or depth or lacking CFHTLS overlap. Particularly the overlapping COSMOS photo- z catalogue of Laigle et al. (2016) is an excellent complement for tests of the influence of photo- z uncertainties (see Cibirka et al. 2016, their Figure 3), which are however not of great relevance to the tests of selection effects in this work.

2.2.1 Spectroscopic samples

A number of spectroscopic samples cover the CFHTLS Deep fields, and we list their details in this section.

The VIMOS VLT Deep Survey (VVDS-Deep, Le Fèvre et al. 2005), with one of its two fields overlapping D1, targets a magnitude-limited sample at $I < 24$. Its overall high spectroscopic completeness (78 per cent with high confidence redshifts) is a strong function of

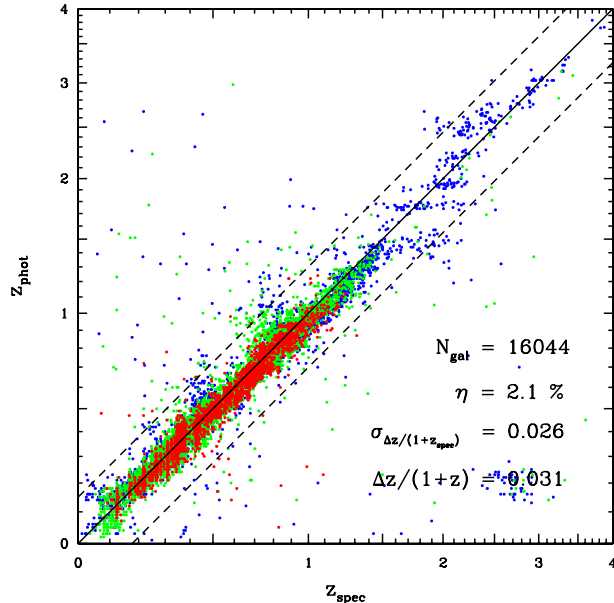


Figure 4. Photometric redshift point estimates of spectroscopic galaxies in CFHTLS Deep compared to their spectroscopic redshifts. The plot shows all galaxies from the VVDS-Deep, VIPERS, zCOSMOS-bright, zCOSMOS-deep, VUDS and DEEP2 spectroscopic surveys with valid CFHTLS Deep and WIRDS photometry in all bands and $i' < 24$. Red, green and blue symbols indicate that the best-fitting templates correspond to early-type, late-type and starburst galaxies in the classification of Dahlen et al. (2005).

apparent magnitude, and decreases especially for $I > 23$, with known colour dependence of the incompleteness (cf. Bonnett et al. 2016, their Fig. 7).

The VIMOS Public Extragalactic Survey (VIPERS, Garilli et al. 2014; Guzzo et al. 2014) is covered by the CFHTLS Wide fields W4 and W1, of which D1 is a pointing. To increase the coverage of galaxies at high redshift, VIPERS uses a $u^*g'r'i'$ colour cut in addition to a $i' < 22.5$ magnitude limit.

zCOSMOS (Lilly et al. 2007) partly overlaps D2 and consists of two separate sub-samples: one (zCOSMOS-bright) magnitude-limited at $I < 22.5$ with ≈ 90 per cent success rate and a second sample (zCOSMOS-deep) of fainter galaxies pre-selected by a colour and B band magnitude limit to be within the redshift range of $1.4 < z < 3.0$.

There are spectra from one pointing of the VIMOS Ultra Deep Survey (VUDS, Le Fèvre et al. 2015; Tasca et al. 2016) in the D2 field. These include very faint objects out to $i' > 25$, which are, however, selected from a complex scheme of colour and photo- z cuts to optimize the yield of high redshift galaxies.

The Deep Extragalactic Evolutionary Probe-2 (DEEP2) survey (Newman et al. 2013) overlaps in part with D3 and, in addition to a magnitude limit at $R < 24.1$, has used cuts in BRI colours to pre-select galaxies with $z > 0.7$.

From all these samples, we use only objects with high-confidence spectroscopic redshifts (quality flag 3 or 4 in the respective catalogue) and include secondary targets that happen to fall inside slit masks.

Table 1. Photometric and spectroscopic samples in the CFHTLS Deep fields after the cuts described in subsection 2.2.

field	phot./spec.	#
D1	phot.	96748
VVDS-Deep	spec.	3187
VIPERS	spec.	1728
D2 (COSMOS)	phot.	130759
zCOSMOS-bright	spec.	3022
zCOSMOS-deep	spec.	904
VUDS	spec.	109
D3	phot.	64003
DEEP2	spec.	3830
D4	phot.	57091

In summary, the only magnitude limited samples (although in a filter that differs slightly from i') overlapping CFHTLS Deep are VVDS-Deep down to $I \approx 23$ and zCOSMOS at $I < 22.5$. DEEP2 and zCOSMOS-deep apply cuts that preferentially reject low-redshift sources, based on B band that is not available from CFHTLS Deep photometry. The expectation is that this cut might bias the spectroscopic sub-sample to higher redshift than a colour-magnitude limited sample based on redder bands only.

3 SELECTION EFFECTS

An idealized empirical method of redshift estimation should return the redshift distribution $p(z|m, c, S)$ of a source estimated under the condition of its observed properties (e.g. colour-magnitude position m, c) and S which encodes selection by additional properties, e.g. position in the sky or other features that influence the success of inclusion in the survey.

For a reference catalogue spanning the colour-magnitude region of interest but observed with a selection function S_{ref} , an empirical algorithm can only be expected to return $p(z) = p(z|m, c, S_{\text{ref}})$ (in the absence of re-weighting). This need not be an issue: for a magnitude-limited reference catalogue and a shallower, magnitude-limited survey, which differ by their footprints in the sky, $S \neq S_{\text{ref}}$ (because of differences in depth and position), yet $p(z|m, c, S_{\text{ref}}) = p(z|m, c, S)$.²

Potentially more harmful is a selection function of the reference catalogue S_{ref} that contains colour-magnitude information not contained in (m, c) (e.g. selection by a band unobserved in the survey or by the success of identifying features in the spectra that allow a certain redshift determination). Likewise, when the reference catalogue is truly magnitude limited but the shallower survey contains only a fraction of objects near the detection limit for which photometric measurements were successful, it is imaginable that $p(z|m, c, S_{\text{ref}}) \neq p(z|m, c, S)$.

In the following sections, we test for selection effects

that significantly change the mean value of β and the redshift distributions of galaxy samples at a fixed (m, c) .

For the latter, in each cell of the colour-magnitude decision tree we compare the distributions of eight-band template-fitting photo- z of two samples, where one has an additional selection effect applied. For testing the selected subsamples for compatibility of their $p(z)$ with the full sample, we run a Cramér-von Mises (CvM) test. When ordering the galaxies in a colour-magnitude box by their photometric redshift point estimate, galaxies with spectroscopic confirmation should be interspersed randomly throughout the list. The CvM statistic T quantifies to which degree this is the case.

For two sets u and v of N and M values (in our case, of photometric redshift) with ranks $u_i, i = 1, \dots, N$ and $v_i, i = 1, \dots, M$ in the ordered, combined set, the CvM statistic T is defined as

$$T = \frac{N \sum_{i=1}^N (\hat{u}_i - u_i)^2 + M \sum_{i=1}^M (\hat{v}_i - v_i)^2}{NM(N+M)} - \frac{4NM-1}{6(N+M)}. \quad (4)$$

In the case that two or more galaxies in our sample share equal redshift (which is common due to the gridded photometric redshift estimates and the fact that, in our tests, one sample is always a subsample of the other), we assign the mean of their combined ranks to all equal redshift objects.

The T statistic for a cell in colour-magnitude space can be interpreted in terms of its p -value, i.e. the probability of finding a value of T higher than what has been found given that u and v are random subsamples from the same population of galaxies. Since the analytical calculation of the p -value is computationally expensive for large sample sizes (Xiao et al. 2006), we use Monte-Carlo realizations of random subsamples to estimate p . This ensures that the p values are uniformly distributed between 0 and 1 for random subsamples of the same size.

3.1 Spectroscopic selection

Selection biases in spectroscopic samples can exist either because the target selection is based on colours not measured in the subset of bands used for the empirical $p(z)$ estimate or because the success of spectroscopic redshift determination depends on properties not fully determined by the photometric information. While these are particularly evident in some cases, e.g. the PRIMUS spectra with a redshift-based selection (Cool et al. 2013) that could not be utilized for the purpose of DES redshift calibration (Bonnett et al. 2016), less obvious spectroscopic selection effects commonly go unchecked.

To test this as robustly as possible, we apply the CvM statistic of Equation 4. We use the same eight-band photo- z estimates of redshift of both samples when comparing the distributions to ensure that disagreement is not due to imperfections in the photo- z . In order to exclude cosmic variance or differences in magnitude calibration as a source of false positives for the disagreement, we run the comparisons individually for each of the spectroscopic samples, using in each case only photometric galaxies from the same CFHTLS Deep pointing.

Given k independent tests (made with independent spectroscopic samples for the same colour-magnitude cell)

² This is only strictly true under the assumption of noiseless m, c and up to cosmic variance.

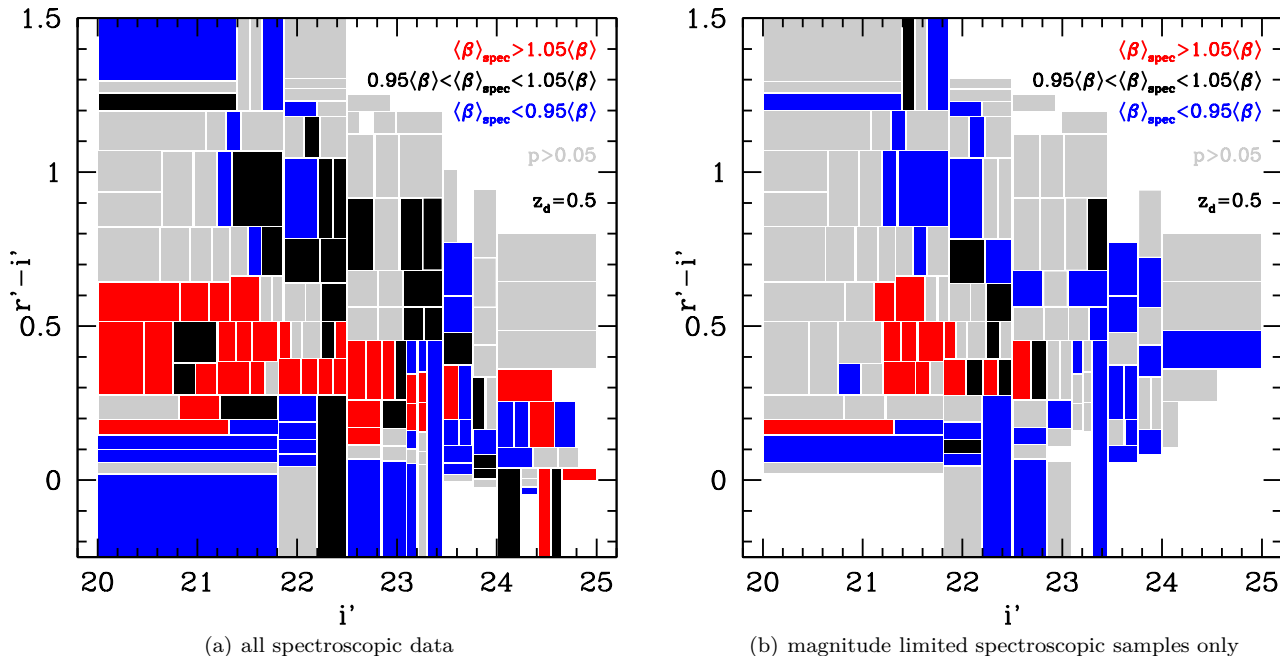


Figure 5. Cramér-von Mises test of $p(z_{\text{phot}})$ of all objects in each colour-magnitude cell vs. the selection of objects for which there is spectroscopic follow-up. Included are cells in $i', r' - i'$ space with at least 10 spectroscopic objects. p -values are calculated for each of the spectroscopic surveys individually on the respective CFHT pointing alone and combined using Equation 5 to avoid cosmic variance. Cells with significant differences in the distributions ($p < 0.05$) are coloured according to the difference in mean β between photometric and spectroscopic objects according to their photometric redshift. *Left-hand panel:* full spectroscopic sample. Cuts at $i' = 22.5$ and 24 have been imposed. *Right-hand panel:* magnitude-limited spectroscopic samples only.

of the same null hypothesis (that the distributions of photo- z of the full sample and spectroscopic subsample agree) that yield p -values p_i , $i = 1, \dots, k$, Fisher's method allows us to combine these into a random variable

$$X = -2 \sum_{i=1}^k \ln p_i. \quad (5)$$

X is χ^2 -distributed with $2k$ degrees of freedom, and the combined p -value of the null hypothesis is $p(\chi_{2k}^2 > X)$.

Figure 5 shows regions in $i', r' - i'$ space for which the null hypothesis is rejected ($p < 0.05$), i.e. where spectroscopic subsamples have different photometric properties in the unused $u^*g'z'JHK_s$ bands that lead to an incompatible photo- z distribution. The disagreement is widespread for the full sample. Limiting the spectroscopic sample to the magnitude limited VVDS-Deep and zCOSMOS-bright samples only, a smaller range of colour-magnitude space shows significant deviations of redshift distributions between the two samples, although there is still clear evidence for selection effects in some regimes. These are likely due to incomplete success of these surveys at faint magnitudes.

While the case of $i', r' - i'$ is useful for illustration, realistic lensing surveys commonly use more than two bands for defining background galaxy samples and estimating redshift distributions. Selection biases on $p(z|c, m, S)$ are reduced in this case, since some of the selection is absorbed from S into c .

Figure 6(a) shows the distribution of p -values of the CvM test in $g'r'i'z'$ and $u^*g'r'i'z'$ colour-magnitude space (as two common example of the many possible combinations

of bands), weighted by the number of galaxies in the respective cell from a magnitude-complete sample at $20 < i' < 25$. While the addition of bands (u^* band in particular) reduces selection effects considerably, a large fraction of galaxies still reside in regions of colour-magnitude space where spectroscopic subsamples are significantly non-representative.

The distribution of residuals in $\langle \beta \rangle$ between full sample and spectroscopic subsample in Figure 6(b) reveals an asymmetric tail towards lower redshift of the spectroscopic subsample.

The overall impact of spectroscopic selection is best described by the (relative) bias on the mean value of β of the spectroscopic subsample relative to the full sample, which would directly correspond to biases on $\Delta\Sigma$ in a lensing analysis that calibrates its source $p(z)$ from spectra. Figure 7 shows this as a function of lens redshift and for two common weighting schemes of source galaxies: one where each source has the same weight in a mean shear analysis (e.g. as in a non-tomographic cosmic shear analysis or in Kwan et al. 2017) and one where sources are weighted by their estimated $\langle \beta \rangle$ for a minimum-variance measurement of $\Delta\Sigma$ (e.g. Sheldon et al. 2004).

The main effect is an underestimation of β , especially for intermediate to large lens redshifts z_d . Minimum-variance weighting by $\langle \beta \rangle_{\text{spec}}$ alleviates (in fact, sometimes overcompensates) the bias by giving less weight (more weight) to parts of colour-magnitude space in which the spectroscopic sample underestimates (overestimates) the mean value of β . In both weightings, however, the bias in β is of problematic amplitude, especially for $z_d > 0.4$. The

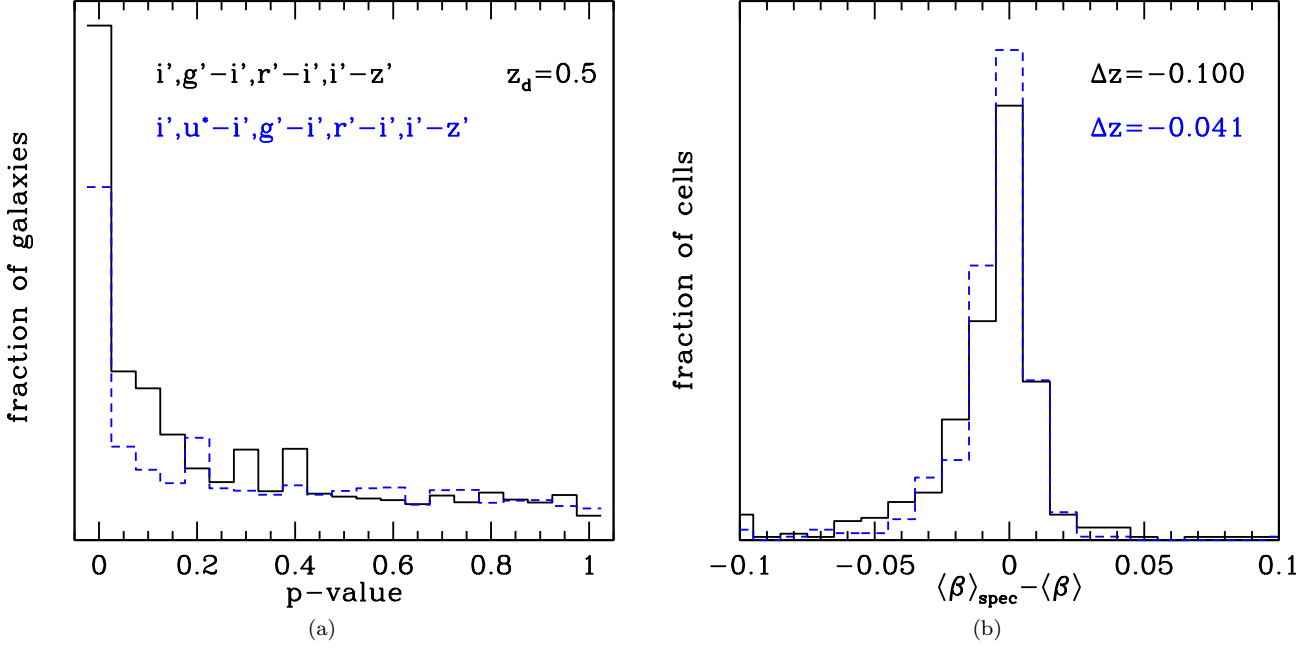


Figure 6. *Left-hand panel:* Histogram of p -values of Cramér-von Mises test comparing the $p(z_{\text{phot}})$ of all objects in each colour-magnitude cell to the selection of objects for which there is spectroscopic follow-up. From the fraction of galaxies lying in cells where $p > 0.5$, we estimate that 30 per cent (43 per cent) of galaxies are represented without selection bias in the spectroscopic catalogues when splitting them by $g'r'i'z'$ ($u^*g'r'i'z'$). Only colour-magnitude cells with at least 10 spectroscopic objects are used. *Right-hand panel:* Histogram of difference in mean β estimated from photometric redshifts of spectroscopic vs. all objects in a colour-magnitude cell.

amplitude of the effect gets somewhat smaller with the addition of u^* band, although the comparison rests on different subsamples due to the exclusion of colour-magnitude cells without spectroscopic galaxies.

We calculate an alternative metric, the mean redshift bias $\Delta z = \langle z \rangle_{\text{spec}} - \langle z \rangle_{\text{all}}$ of all galaxies in the magnitude-limited sample from cells with at least one spectroscopic object. For $u^*g'r'i'z'$ ($g'r'i'z'$) and the colour-magnitude decision tree generated for $z_d = 0.5$, we find $\Delta z = 0.839 - 0.880 = -0.041$ (-0.100 , respectively), at levels exceeding the requirements of ongoing lensing surveys (e.g. Samuroff et al. 2017).

Importantly, these selection biases cannot be corrected by any weighting scheme that is based on the observed magnitudes in a $(u^*)g'r'i'z'$ survey: even at the same observed colour-magnitude (i.e. in one colour-magnitude cell), the redshift distributions of spectroscopic and full sample differ.

We note that these results are found with the underlying assumption that the eight-band photometric redshifts from the CFHTLS and WIRDS photometry are the *true* redshifts of the galaxies in our reference sample. Spectroscopic and magnitude-limited samples differ in their eight-band template-fitting $p(z)$, e.g. in a $g'r'i'z'$ colour-magnitude cell. This means that in that cell, the distribution of the remaining u^*JHK_s magnitudes of the two samples differ in a way that impacts the template fitting. This is a conservative definition for the purpose of detecting selection effects: additional spectroscopic selection effects that are not recognizable with this set of 8 filters or the templates used are possible. Our comparison of the CFHTLS eight-band with

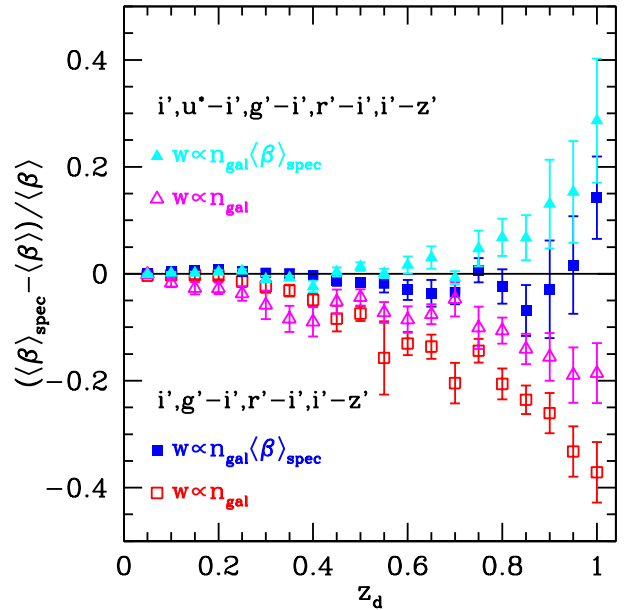


Figure 7. Relative bias in mean β (i.e. in estimated $\Delta\Sigma$) between spectroscopic subsample and magnitude-limited source sample at $20 < i' < 25$. Blue (cyan) filled square (triangle) symbols and red (magenta) open symbols show minimum variance lensing weighting and uniform weighting of colour-magnitude cells in $g'r'i'z'$ ($u^*g'r'i'z'$), respectively. Cells without spectroscopic galaxies are excluded from the source sample.

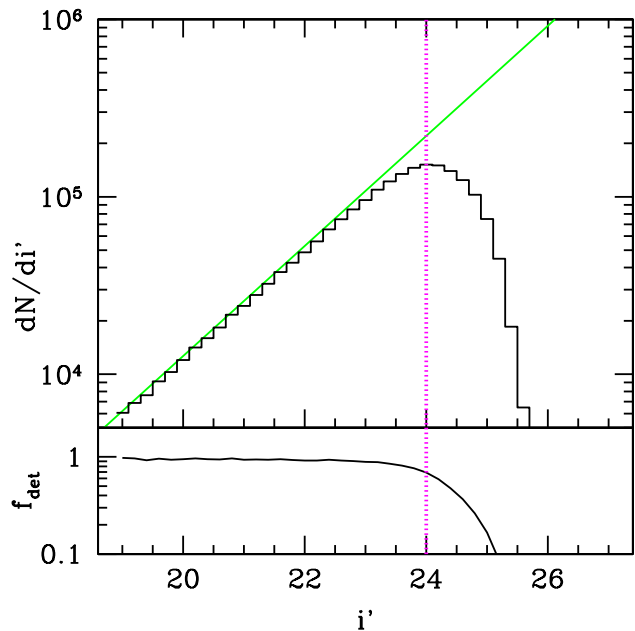


Figure 8. Upper panel: Distribution of apparent i' band magnitude of galaxies detected in the CFHTLS Deep fields after adding Gaussian noise as described in the text. Green line indicates a power-law fit to the full photometric sample in the range $19 < i' < 22$. Lower panel: Completeness of object detection is estimated relative to the power-law fit. Vertical line indicates the peak of the histogram at $i'_t = 24$. For comparison the figure is shown with the same axis scaling as Figure 2.

spectroscopy and COSMOS 36-band photometric redshifts (Laigle et al. 2016) in Cibirka et al. (2016) indicates, however, that in most of colour-magnitude space the eight-band information is sufficient for highly accurate redshift estimation.

3.2 Photometric incompleteness

Faint sources near the detection limit dominate the background galaxy samples in contemporary imaging surveys, in terms of their number and their contribution to lensing signal-to-noise. To reach sufficient background galaxy number densities for weak lensing studies, it is typically necessary to include sources at magnitudes where the completeness is below unity. As an example, Applegate et al. (2014) apply a relatively conservative cut at the magnitude m_t where dN/dm turns over. In the photometric reference catalogue we use, however, for a cut at magnitudes $\approx m_t - 1$ or fainter, the sample is not truly magnitude limited.

In addition to random noise, other galaxy parameters (such as, e.g., size or morphology) might influence the detection probability of a source. If these parameters correlate with source redshift, the recovered source population might have a $\langle\beta\rangle$ that differs from the value of a truly magnitude limited sample to which the same colour-magnitude cuts have been applied. Because fields used for photometric measurements on reference samples of galaxies are (ideally) deeper, photometric selection effects will be weaker or nonexistent for the reference samples, potentially causing a bias.

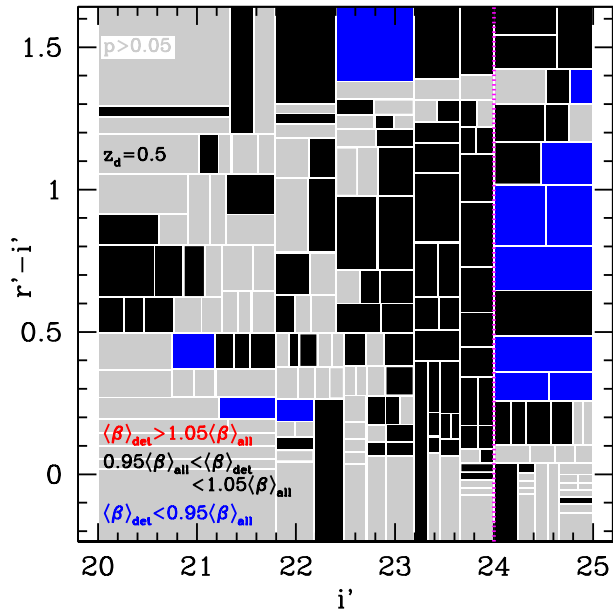


Figure 9. CvM test of $p(z_{\text{phot}})$ of all objects vs. objects detected in images to which noise was added such that the magnitude distribution dN/di' peaks at $i'_t = 24$ (indicated by magenta vertical, dashed line). Cells with significant differences in the distributions ($p < 0.05$) are coloured according to the difference in mean β between all objects and objects recovered from the noisy data according to their photometric redshift derived from the deep data.

We test this by adding noise to our CFHTLS Deep reference field images and re-running the photometric pipeline used to generate the magnitude limited reference catalogues. To this end, we use SExtractor background noise maps to determine the noise present in each pixel. We then add uncorrelated Gaussian noise to each pixel, such that the sum of the original variance and the variance of the artificial noise match a constant value for each of the CFHT pointings, chosen to have equal signal-to-noise in the aperture flux measurement of sources of the same extinction corrected flux in each of the pointings. We then re-run our object extraction, using a background noise map that is a constant at the respective value, masking a small number of pixels for which the original background noise already was above the target noise level. We chose the overall level of noise such that the magnitude histogram of the recovered sources peaks at $i'_t = 24$ (cf. Figure 8). In the resulting catalogue, the completeness is $\approx 75\%$ at $i'_t = 24$ and only $\approx 20\%$ at $i' = 25$, the completeness limit of the original data.

Figure 9 shows the results of a CvM test of the $p(z)$ of the magnitude-limited vs. the detected subsample in $i', r' - i'$ space. Due to the much larger number of galaxies, small differences in the $p(z)$ of each colour-magnitude box can be detected with high significance. Such differences are present, especially at $i' > 23$ (one magnitude brighter than the turnover of dN/di'). The difference of mean $\langle\beta\rangle$ is, however, far below the 5 per cent level in this regime. At the highly incomplete tail of $i' > 24$, we find that the galaxies recovered from the noise tend to be at lower redshift, causing a considerable bias of β .

Figure 10 summarizes at the mean bias as a function of

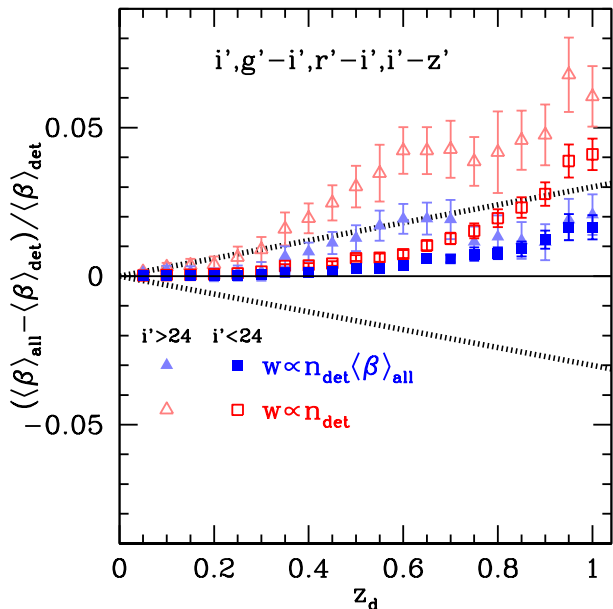


Figure 10. Relative bias in mean β (i.e. in estimated $\Delta\Sigma$) between magnitude-limited source sample at $20 < i' < 25$ and subsample detected in noisy data with peak of the magnitude distribution dN/di' at $i'_t = 24$. Blue filled symbols and red open symbols show minimum variance lensing weighting and uniform weighting of colour-magnitude cells in $g'r'i'z'$, respectively. Rectangular symbols show bright sample at $i' < 24$, while faint, triangular symbols show cells with $i' > 24$. The dotted, thick black lines indicate the approximate level of cosmic variance of lensing-weighted mean β from the CFHTLS Deep reference catalogue (cf. Appendix B).

lens redshift for $g'r'i'z'$ information³, split by source magnitude. Using only galaxies on the bright side of the turn-over point, $i' < 24$, biases in optimally weighted source samples are always below the 2 per cent level. Biases in unweighted samples are larger, yet also at or below that level except for high lens redshift. Biases for the faint sample are only mildly worse in the weighted case, yet reach 5 per cent in the unweighted analysis at $z_d > 0.5$. While there is a clear detection of selection bias, we note that cosmic variance from the limited number of four CFHTLS Deep reference fields (approximated by $\sigma_\beta/\beta \approx 0.03z_d$, cf. Appendix B) is comparable to or larger than the bias caused by detection selection in the noisy data. The expected, even lower per cent level statistical uncertainty e.g. for lensing mass calibration of optical cluster samples in final DES data, implies that both a treatment of this selection bias and an expansion of reference catalogues to reduce cosmic variance will be necessary.

3.3 Shape measurement incompleteness and weighting

Weak lensing shape catalogues of galaxies suffer another significant step of selection during star-galaxy separation and

³ The result is qualitatively independent of the combination of bands used

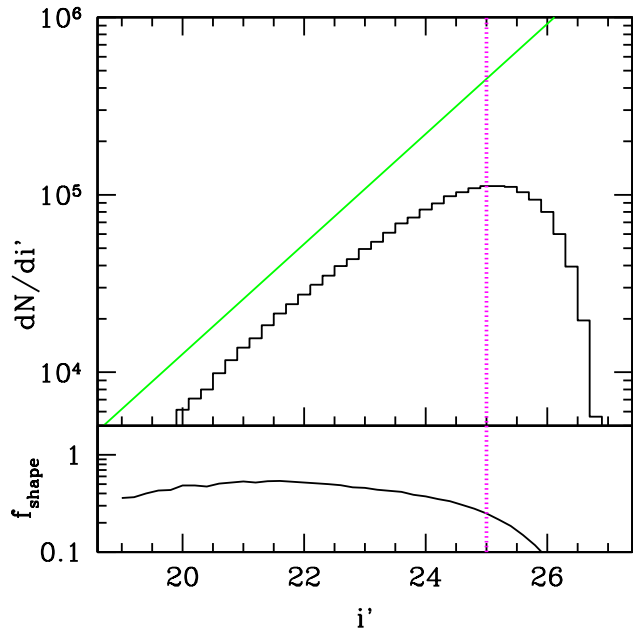


Figure 11. Upper panel: Distribution of apparent i' band magnitude of galaxies with successful shape measurement in the CFHTLS Deep fields. Green line indicates power-law fit to full photometric sample in the range $19 < i' < 22$ (cf. Figure 2). Lower panel: Completeness of shape catalogue relative to the power-law fit. Magenta lines indicates turnover magnitude $i' = 25$, which is also the magnitude completeness limit of the photometric input catalogue. For comparison the figure is shown with the same axis scaling as Figure 2.

shape measurement. We investigate the effect of this on redshift biases by running a shape measurement pipeline on the CFHTLS Deep i' band images and comparing the recovered to the full sample.

To this end, we perform a simple galaxy selection by a size cut above the stellar sequence (cf., e.g. Gruen et al. 2013, their fig. 7), measure the shapes of galaxies with an implementation of the Kaiser, Squires, & Broadhurst (1995) algorithm, and apply cuts in shear responsivity, S/N of the shape measurement, and ellipticity (as in Gruen et al. 2014, their section 4.2).

The resulting sample not only is somewhat shallower than the underlying magnitude-complete sample (see Figure 11), but also excludes a considerable fraction of brighter galaxies due to the size and responsivity cuts. We note that while the exact selection certainly differs between shape measurement pipelines, this qualitative observation generally holds (cf., e.g., Jarvis et al. 2016, their Fig. 29). The question is to what degree this morphology based selection changes the redshift distribution of the sample (see e.g. Applegate et al. 2014, who find biases at the few per cent level from approximating shape catalogue selection by a size cut).

Figure 12 shows the result of a CvM test of the compatibility of the $p(z_{\text{phot}})$ of the magnitude complete sample and the shape catalogue subsample in cells in $i', r' - i'$. Significant differences in the redshift distributions are detected in large parts of colour-magnitude space. There appears to be a qualitative difference between the brighter subsample

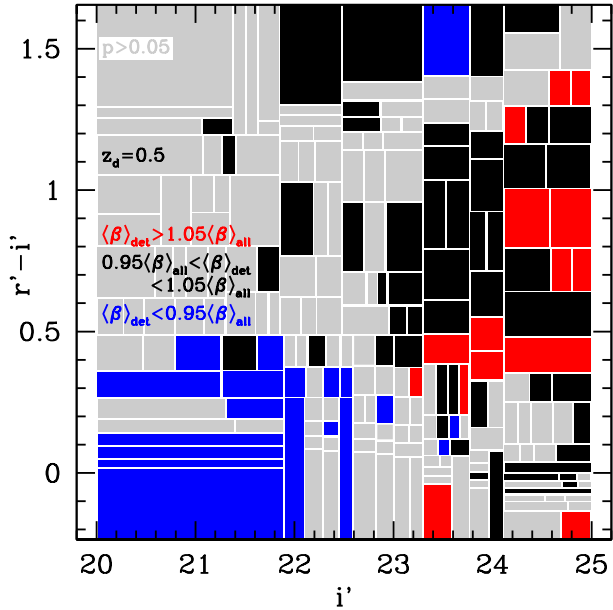


Figure 12. CvM test of $p(z_{\text{phot}})$ of all objects vs. objects with successful shape selection and measurement. Cells with significant differences in the distributions ($p < 0.05$) are coloured according to the difference in mean β between all objects and objects recovered from the noisy data according to their photometric redshift derived from the deep data.

at $i' < 23$, for which objects with successful shape measurement tend to be at lower redshift, and the faint subsample at $i' > 23$, where the opposite is the case.

For this reason, we investigate the impact of the shape selection on $\Delta\Sigma$ for the bright and faint samples separately in Figure 13. The bias of each sample is significant, but small compared to both the biases of spectroscopic selection described in subsection 3.1 and the cosmic variance from using only the four CFHTLS Deep fields for $p(z)$ estimation. This is especially true for the combination of bright and faint sample, in which the opposite effects partially cancel each other. At the 1-2 per cent level of relative error, shape selection remains a relevant factor, especially with future surveys that intend to use larger reference catalogues for reducing cosmic variance.

We also test the effect of weighting sources by their shape noise inverse variance, as it is commonly done to maximize S/N in weak lensing analyses. We find that the effect of this weighting on selection-based redshift biases is small compared to the above effect. Because the shape noise is strongly dominated by intrinsic dispersion of galaxy shapes in the case of CFHT Deep, where measurement noise is typically small, this conclusion could conceivably be different in more noisy data.

4 CONCLUSIONS

We have developed a scheme for testing the impact of selection biases on empirical (training-based) $p(z)$ estimation methods for the purpose of weak lensing $\Delta\Sigma$ analyses. To this end, we use a reference catalogue with high-quality

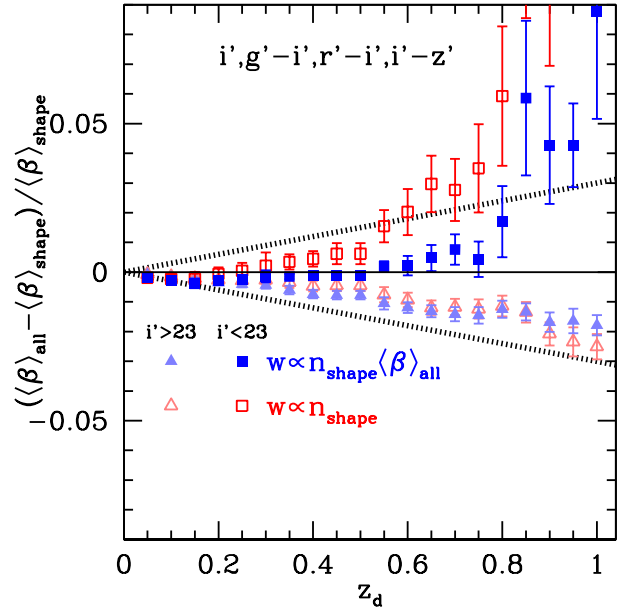


Figure 13. Relative bias in mean β (i.e. in estimated $\Delta\Sigma$) between magnitude-limited source sample at $20 < i' < 25$ and subsample selected for and successful in shape measurement. Blue filled symbols and red open symbols show minimum variance lensing weighting and uniform weighting of colour-magnitude cells in $g'r'i'z'$, respectively. Rectangular symbols show bright sample at $i' < 23$, while faint, triangular symbols show cells with $i' > 23$. The dotted, thick black lines indicate the approximate level of cosmic variance of lensing-weighted mean β from the CFHTLS Deep reference catalogue (cf. Appendix B).

template-fitting photometric redshift point-estimates from CFHTLS Deep optical and WIRDS near-infrared broadband photometry. To mimic empirical $p(z)$ estimation, we use a decision tree algorithm based on subsets of the available bands. We then apply this algorithm to estimate the $p(z)$ of galaxies in the reference catalogue itself as a target sample. In this, we impose selection effects and test their impact in terms of differences between the true and estimated distributions of z_{phot} of the target sample.

Selection effects in existing spectroscopic subsamples are significant over large parts of colour-magnitude space (cf. subsection 3.1, Figure 5). The dominant trend is that the existing spectroscopic subsamples are biased towards lower redshift than complete samples of equal magnitude and colour. Therefore the uniformly weighted mean z and D_{ds}/D_s estimated by empirical methods that rely on these spectroscopic training samples (Fig. 6) are also biased low, the latter at the 10 per cent level for moderate lens redshifts (Figure 7, open symbols). Because some parts of colour-magnitude space show opposite biases (Fig. 5), an optimally weighted $\Delta\Sigma$ measurement partially compensates the D_{ds}/D_s offset (Fig. 7, filled symbols). Because the redshift distributions of magnitude limited and spectroscopic subsamples at the same observed colour-magnitude differ, no re-weighting as a function of observed (photometric) galaxy properties can remedy these selection biases.

Even with an optimal, magnitude-limited reference catalogue, selection biases in the lensing source catalogue

due to object detection from noisy data and incomplete, morphology dependent success of shape measurement and star-galaxy separation can change the $p(z)$ distribution of the source sample. We test both of these effects (cf. subsection 3.2 and 3.3) and find them to be significant, although at a lower level than the aforementioned spectroscopic selection biases (cf. Figure 10 and 13). For the most common use cases ($\Delta\Sigma$ weighted measurements, lens redshifts below $z_d = 0.8$) these selection biases are below the typical level of cosmic variance due to only having four square-degree reference fields of CFHTLS Deep data. For future surveys that use larger reference catalogues for reducing cosmic variance, these effects may, however, be relevant. In order to improve beyond 2 per cent level accuracy, empirical photo- z methods will require both an increase in the number of reference fields and a treatment of selection effects in shape catalogues.

The dominant selection biases for empirical $p(z)$ estimation at this point therefore are due to target selection and incompleteness in the reference spectroscopic surveys. There are a number of potential avenues to address this issue:

- Masters et al. (2015) suggest the observation of representative spectroscopic samples over all relevant parts of colour-magnitude space, as defined by a self-organizing map (SOM). *Representativeness* of the spectroscopic catalogue means two things: (1) sampling all of colour-magnitude space (as can be ensured by targeting galaxies in unpopulated cells of the SOM), and (2) ensuring that at a given colour-magnitude position there is no redshift dependence of spectroscopic incompleteness. We note that our tests of existing spectroscopic samples with claimed magnitude-limited target selection reveal non-negligible selection effects (cf. Figure 5b), likely due to residual incompleteness of these surveys towards the faint end of their galaxy samples. Similar tests could be run on cells of the SOM.

- Redshifts from angular cross-correlation of source galaxies with overlapping samples of known redshift do not require representative coverage with spectroscopic follow-up (see e.g. Schneider et al. 2006; Newman 2008; Schmidt et al. 2013; Ménard et al. 2013 and the recent application for cross-validation of the KiDS lensing $p(z)$ Hildebrandt et al. 2017; Morrison et al. 2016). In addition, the method automatically accounts for selection effects in lensing source catalogues. These advantages make clustering redshifts a promising approach for future large-area surveys. Caveats include the requirement of moderately large samples of tracers with known z out to large redshift, potential systematics from calibrating galaxy bias as a function of redshift (e.g. Newman et al. 2015, their section 3.1), and the need for a combined likelihood for cosmological parameters and $p(z)$ constrained from a joint data vector (including e.g. lensing and galaxy clustering) and the measurements made for clustering redshifts.

- A Bayesian scheme of fully representative galaxy templates and appropriate priors would allow for optimal $p(z)$ estimation from photometric data. While it is not evident how such a template set could be derived from a priori considerations or sparse spectroscopic surveys, a hierarchical Bayesian scheme such as that of Leistedt et al. (2016) could potentially derive coarse templates and priors along with $p(z)$ from survey data (see also Benítez 2000, for estimating

priors from the data). In order to break degeneracies of type and redshift in broad-band photometry, it might be necessary to include subsamples with narrow-band photometry or spectra in the hierarchical inference.

- Surveys with numerous, narrow bands such as the Alhambra (Moles et al. 2008), PAU (Martí et al. 2014) and J-PAS (Benítez et al. 2014) surveys, are in the process of deriving photometric redshifts with small uncertainties and outlier rates for large, magnitude-limited samples of galaxies. These samples might be well suited for empirical $p(z)$ estimation, although care must be taken to account for weak lensing source catalogue level selection at the few per cent level of systematic uncertainty.

There are thus multiple pathways to improve $p(z)$ estimation for the purpose of weak lensing. A framework like the one presented in this paper can provide a straightforward way of exploring those.

ACKNOWLEDGEMENTS

This work is based on data made public by the CFHT Legacy Survey and the DEEP2, VIPERS, VUDS, VVDS-Deep and zCOSMOS spectroscopic surveys. The authors thank Steve Allen, Douglas Applegate, Nathalia Cibirka, Alexis Finoguenov, Enrique Gaztañaga, Will Hartley, Ben Hoyle, Ofer Lahav, Anja von der Linden, Peter Melchior, Anna Ogorzalek, Eduardo Rozo, Risa Wechsler, the anonymous referee and the DES and LSST photo- z working groups for helpful discussions.

Support for DG was provided by NASA through the Einstein Fellowship Program, grant PF5-160138.

APPENDIX A: STATISTICAL UNCERTAINTY OF LENSING RECONSTRUCTION

In this appendix, we derive expressions for how the signal-to-noise ratio (S/N) of the lensing measurement is diminished when source galaxies are selected and weighted by their estimated redshift distribution rather than their true redshifts, using different combinations of filter bands. Results are given for deep ($i' < 25$) and shallower ($i' < 24$) samples for all permutations of 2-4 band $g'r'i'z'$ photometry, in the hope that they might be useful in designing photometric surveys.

For a set of sources $s = 1, \dots, N$ with true β_s relative to some lens redshift z_d , the optimal estimator of gravitational shear combines the shears of all sources with a weight $w_s \propto \beta_s/\sigma_s^2$, where σ_s contains intrinsic and measurement related noise in the shape of source s . This relative weighting corresponds to the common $\Delta\Sigma$ estimator (e.g. Sheldon et al. 2004).

Let the tangential shear for source s be $\gamma_s = \beta_s\gamma$, assume $\sigma_s = \sigma_\gamma$ is equal for all sources, and set $w_s = \beta_s/\sigma_\gamma^2$. The signal-to-noise ratio of the weighted estimate of γ is

$$\frac{S}{N} = \frac{\sum \beta_s \gamma \times \beta_s / \sigma_\gamma^2}{\sqrt{\sum \sigma_\gamma^2 \times \beta_s^2 / \sigma_\gamma^4}} = \frac{\gamma}{\sigma_\gamma} \sqrt{\sum \beta_s^2} \quad (\text{A1})$$

If instead of the true value of β_s we only have an esti-

mate $\hat{\beta}_s$, the S/N becomes

$$\frac{S}{N} = \frac{\sum \beta_s \gamma \times \hat{\beta}_s / \sigma_\gamma^2}{\sqrt{\sum \sigma_\gamma^2 \times \hat{\beta}_s^2 / \sigma_\gamma^4}} = \frac{\gamma}{\sigma_\gamma} \frac{\sum \hat{\beta}_s \beta_s}{\sqrt{\sum \hat{\beta}_s^2}}. \quad (\text{A2})$$

If the overall sample of N galaxies is split into subsamples j with N_j galaxies each, and we have calibrated $\langle \beta \rangle_{s \in j}$ and assign it to each galaxy in the subsample (precisely what is done by our decision tree method), then

$$\frac{S}{N} = \frac{\gamma}{\sigma_\gamma} \frac{\sum_j N_j \langle \beta \rangle_{s \in j}^2}{\sqrt{\sum_j N_j \langle \beta \rangle_{s \in j}^2}} = \frac{\gamma}{\sigma_\gamma} \sqrt{\sum_j N_j \langle \beta \rangle_{s \in j}^2}. \quad (\text{A3})$$

For the simple case of a single sample with constant β estimate, $\hat{\beta}_s = \langle \beta \rangle$, this reduces to

$$\frac{S}{N} = \frac{\gamma}{\sigma_\gamma} \frac{\sum \langle \beta \rangle^2}{\sqrt{\sum \langle \beta \rangle^2}} = \frac{\gamma}{\sigma_\gamma} \sqrt{\sum \langle \beta \rangle^2}. \quad (\text{A4})$$

It therefore makes sense to define a metric that quantifies the fraction of the S/N ratio recovered when using $\hat{\beta}$ instead of β as

$$\text{rel. S/N} = \frac{\sqrt{\sum_j N_j \langle \beta \rangle_{s \in j}^2}}{\sqrt{\sum \beta_s^2}} = \sqrt{\frac{\langle \langle \beta \rangle_{s \in j}^2 \rangle_j}{\langle \beta_s^2 \rangle_s}}, \quad (\text{A5})$$

where the average over subsamples $\langle \dots \rangle_j$ weights each subsample by its population N_j .

Figure 1 shows the relative S/N recovered in each colour-magnitude box based on the metric of the above equation by the colour saturation of the box lines drawn. Figure A1 shows the relative S/N of magnitude-limited samples from a colour-magnitude decision tree in all combinations of i' and $u^*g'r'z'$.

While some combinations of two photometric bands do not recover much of the signal-to-noise lost by using the full sample with uniform weight (black lines), three-band (four-band) surveys consistently recover all but $30 \times z_d$ per cent ($20 \times z_d$ per cent) of the optimally weighted information. A similar statement can be made about tomographic cosmic shear analyses with colour-cut subsamples (Jain et al. 2007). We note, however, that also cosmic variance is a fairly strong function of the number and selection of bands used (see Appendix B), and therefore samples selected with fewer bands require larger reference catalogues.

APPENDIX B: COSMIC VARIANCE

Cosmic variance enters β estimation from photometry because photometry does not uniquely constrain a galaxy's redshift. The matter (and galaxy) density of a reference field as a function of redshift therefore influences the estimated $p(z)$ of a given galaxy from comparison to the reference sample. The level of cosmic variance, e.g. expressed in terms of the relative systematic uncertainty of β , decreases with the number and area of reference fields used and the discriminating power of the photometric information.

To determine the level of cosmic variance in our reference catalogues, we calculate Jackknife uncertainties for the estimated value of $\langle \beta \rangle$ for a lensing-weighted sample from splitting the reference catalogue into the four CFHTLS Deep fields. We build a decision tree as before, based on

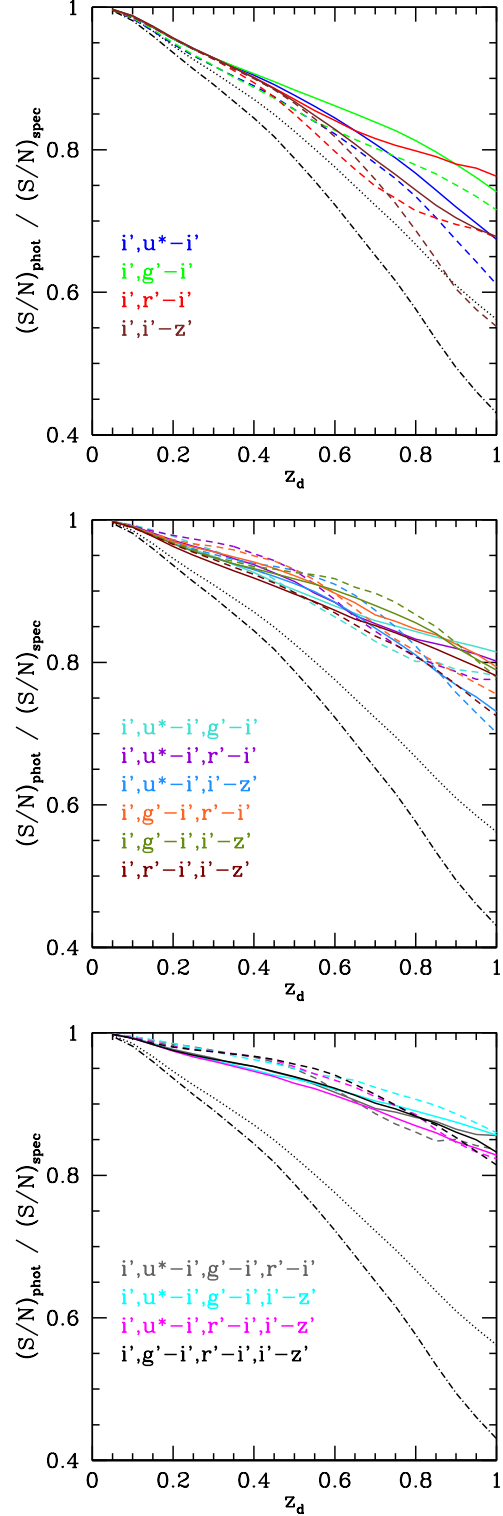


Figure A1. Loss in lensing S/N relative to background selection and weighting from spectroscopic redshifts for β estimated from a decision tree with 2, 3 or 4 band photometric information (top, central and bottom panel) as a function of lens redshift z_d . Solid (dashed) lines indicate the case of $20 < i' < 25$ ($20 < i' < 24$) source galaxies. Black dotted (dotted-dashed) lines show the loss in S/N in the case of assigning equal lensing weight to all sources.

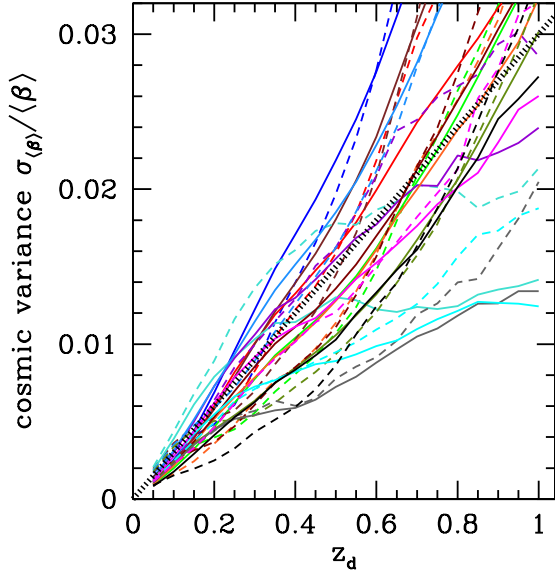


Figure B1. Relative cosmic variance of the lensing-weighted value of β of a sample of galaxies with $20 < i' < 25$ (solid lines) and $20 < i' < 24$ (dashed lines) when estimated from the four CFHTLS Deep fields. Color coding of the different combinations of bands is as in Figure A1. Thick, dotted line indicates $\sigma_{\langle\beta\rangle}/\langle\beta\rangle = 0.03 \times z_d$.

all sources. The value of $\langle\beta\rangle_j$ is calculated for each colour-magnitude box j from the jackknifed subsample of reference objects. Color-magnitude boxes are weighted by the number and mean value of β of objects in the full catalogue. We convert the jackknife uncertainty $\sigma_{\langle\beta\rangle}$ of the weighted mean $\langle\beta\rangle$ to a relative uncertainty $\sigma_{\langle\beta\rangle}/\langle\beta\rangle$.

Results are shown in Figure B1 and indicate that, for a reference catalogue made of four independent square-degree pointings with the level of calibration homogeneity achieved for CFHTLS Deep, the relative level of cosmic variance is an approximately linear function of lens redshift, where suitable combinations of bands achieve $3\% \times z_d$ or better while less optimal choices yields $\approx 5\% \times z_d$. A larger number of photometric bands typically allow for lower cosmic variance, down to $1.5\% \times z_d$. The most favorable combinations of bands generally include u^* band data. These results appear to be only a mild function of the depth of the sample.

For a reference catalogue compiled from N_{fields} independent square-degree fields, these uncertainties should scale as $\sqrt{4/N_{\text{fields}}}$.

APPENDIX C: MAGNIFICATION BIAS

If a galaxy is re-mapped by a lensing Jacobian A , its surface area and observed flux increase by a magnification factor $\mu = \det A^{-1}$, which in the weak limit is approximated as $\mu \approx 1 + 2\kappa$. At the same time, the surface number density of galaxies of these intrinsic properties decreases to μ^{-1} of its un-lensed value. Due to these two competing effects, the detected number density of galaxies in a magnitude limited sample can either increase or decrease. For a population with

log-normal luminosity function $n(m)$ at the faint end with $d \log n(< m)/dm = s$, the change in number density is approximately $\Delta n/n = (5s - 2)\kappa$ (e.g. Broadhurst et al. 1995; Umetsu et al. 2011).

Because s depends on galaxy type and $\kappa \propto \beta$ depends on source redshift, magnification changes the colour-magnitude distribution and $p(z)$ of the observed galaxy population. In this Appendix, we study two aspects of that with the decision tree scheme:

- the difference between the estimated $\langle\beta\rangle_{\text{est}}$ and the true $\langle\beta\rangle_{\text{true}}$ of the magnified, magnitude limited population; this can be thought of as an effect of the prior in redshift, type and luminosity being wrong when estimated from the field population of a reference catalogue but applied to a magnified population
- the difference between the estimated $\langle\beta\rangle_{\text{est}}$ of a magnified population and the estimated field value $\langle\beta\rangle_{\text{field}}$ of an unmagnified sample with the same magnitude limits; this is of importance when differences in estimated $p(z)$ between the field population and galaxy samples around clusters are used to estimate the contamination of the lensing source sample with cluster member galaxies (e.g. for the purpose of estimating lensing boost factors, see Melchior et al. 2016, their section 4.2)

To this end, we apply magnification to the reference catalogues and process them with a decision tree build on the un-magnified reference catalogue. Our methodological choices in this case are

- to consider a magnitude-limited sample (both in the magnified and unmagnified case) of $20 < i' < 24$, comparable to lensing source catalogues of ongoing large-area surveys;
- to build a decision tree as described in subsection 2.1, with a minimum number of 1000 reference sources per $g'r'i'z'$ colour-magnitude box;
- to apply magnification due to a lens at some z_d with $\kappa = 0.1$ for sources at a hypothetical $\beta = 1$; we ensured that the effect is well-described as linear in $\kappa(\beta)\beta^{-1}$ in the weak regime and describe the result as a relative change in $\langle\beta\rangle$ per unit $\kappa(\beta)\beta^{-1}$;
- and to model magnification as a magnitude shift $\Delta m = -2.5 \log(1 + 2\kappa)$, which moves some galaxies to different colour-magnitude boxes, and a rarefaction that corresponds to a relative weight of $w = (1 + 2\kappa)^{-1}$ of each galaxy

We estimate the respective versions of β in a $\Delta\Sigma$ fashion, i.e. weighting each colour-magnitude box j by $N_j \langle\beta\rangle_{j,\text{field}}$.

We show the results of this test in Figure C1. An example to read off from the plot is that for a lens at $z_d = 0.6$ with a convergence of $0.1 \times \beta$, the estimated $\langle\beta\rangle$ of a magnified background population with observed $20 < i' < 24$ is about 1 per cent smaller than the true $\langle\beta\rangle$, and about 1 per cent larger than the mean $\langle\beta\rangle$ of a field sample in this magnitude range.

These effects can affect cluster mass estimation with weak lensing in three ways:

- The underestimation of the β of the magnified population causes an overestimate of mass, yet at an even smaller amplitude due to the much smaller convergence at larger

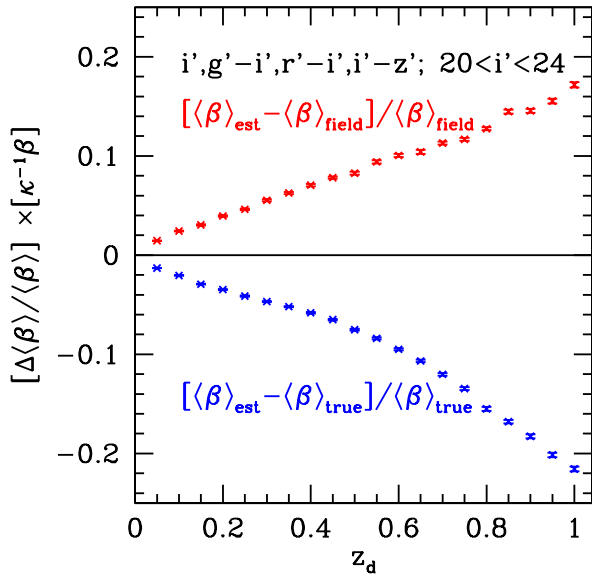


Figure C1. Influence of lensing magnification of the background population on $\langle\beta\rangle$ estimates in a sample selected by observed magnitude $20 < i' < 24$. We show the relative bias due to mismatch between the field prior, $\langle\beta\rangle_{\text{est}} - \langle\beta\rangle_{\text{field}}$ of the magnified population (blue, always < 0) and the *estimated* relative difference $\langle\beta\rangle_{\text{est}} - \langle\beta\rangle_{\text{true}}$ between the magnified and unmagnified population (red, always > 0) as a function of lens redshift, for a hypothetical $\kappa = 1$ at $\beta = 1$.

radii from the cluster center, where most of the constraining power of the shear signal is located.

- The effect via boost factors estimated from $p(z)$ decomposition (Gruen et al. 2014, their section 3.1.3 and Melchior et al. 2016, their section 4.2) is a likely underestimate of background contamination (because the presence of cluster members should decrease the estimated $\langle\beta\rangle$, opposite to the effect of magnification) that causes an opposite bias of comparable amplitude.

- For boost factors estimated from the number density of background sources, the effect will be opposite. For lenses at $0.4 < z_d < 1.0$, we find that the magnified sample in $20 < i' < 24$ has a higher surface density by $\approx \kappa\beta^{-1} \times 10$ per cent from magnification. This will bias boost factors high and, as a result, masses high.

REFERENCES

Applegate D. E. et al., 2014, *Mon. Not. Roy. Astron. Soc.*, 439, 48
 Arnouts S., Cristiani S., Moscardini L., Matarrese S., Lucchin F., Fontana A., Giallongo E., 1999, *Mon. Not. Roy. Astron. Soc.*, 310, 540
 Bartelmann M., Schneider P., 2001, *Physics Reports*, 340, 291
 Bender R. et al., 2001, in *Deep Fields*, Cristiani S., Renzini A., Williams R. E., eds., p. 96
 Benítez N., 2000, *ApJ*, 536, 571
 Benítez N. et al., 2014, *arXiv:1403.5237*

Bertin E., Arnouts S., 1996, *A&AS*, 117, 393
 Bielby R. et al., 2012, *A&A*, 545, A23
 Bonnett C. et al., 2016, *Phys. Rev. D*, 94, 042005
 Brammer G. B., van Dokkum P. G., Coppi P., 2008, *ApJ*, 686, 1503
 Brimiouille F., Seitz S., Lerchster M., Bender R., Snigula J., 2013, *Mon. Not. Roy. Astron. Soc.*, 432, 1046
 Broadhurst T. J., Taylor A. N., Peacock J. A., 1995, *ApJ*, 438, 49
 Carrasco Kind M., Brunner R. J., 2013, *Mon. Not. Roy. Astron. Soc.*, 432, 1483
 Cibirka N. et al., 2016, *ArXiv e-prints*
 Collister A. A., Lahav O., 2004, *PASP*, 116, 345
 Connolly A. J., Csabai I., Szalay A. S., Koo D. C., Kron R. G., Munn J. A., 1995, *AJ*, 110, 2655
 Cool R. J. et al., 2013, *ApJ*, 767, 118
 Dahlen T., Mobasher B., Somerville R. S., Moustakas L. A., Dickinson M., Ferguson H. C., Giavalisco M., 2005, *ApJ*, 631, 126
 Erben T. et al., 2005, *Astronomische Nachrichten*, 326, 432
 Firth A. E., Lahav O., Somerville R. S., 2003, *Mon. Not. Roy. Astron. Soc.*, 339, 1195
 Garilli B. et al., 2014, *A&A*, 562, A23
 Gruen D. et al., 2013, *Mon. Not. Roy. Astron. Soc.*, 432, 1455
 Gruen D. et al., 2014, *Mon. Not. Roy. Astron. Soc.*, 442, 1507
 Guzzo L. et al., 2014, *A&A*, 566, A108
 Heymans C. et al., 2012, *Mon. Not. Roy. Astron. Soc.*, 427, 146
 Hildebrandt H. et al., 2006, *A&A*, 452, 1121
 Hildebrandt H. et al., 2017, *Mon. Not. Roy. Astron. Soc.*, 465, 1454
 Hoyle B., 2016, *Astronomy and Computing*, 16, 34
 Hoyle B., Rau M. M., Zitlau R., Seitz S., Weller J., 2015, *Mon. Not. Roy. Astron. Soc.*, 449, 1275
 Ilbert O. et al., 2006, *A&A*, 457, 841
 Ilbert O. et al., 2009, *ApJ*, 690, 1236
 Jain B., Connolly A., Takada M., 2007, *J. Cosmol. Astropart. Phys.*, 3, 013
 Jarvis M. et al., 2016, *Mon. Not. Roy. Astron. Soc.*, 460, 2245
 Kaiser N., Squires G., Broadhurst T., 1995, *ApJ*, 449, 460
 Kuijken K. et al., 2015, *Mon. Not. Roy. Astron. Soc.*, 454, 3500
 Kwan J. et al., 2017, *Mon. Not. Roy. Astron. Soc.*, 464, 4045
 Laigle C. et al., 2016, *ApJS*, 224, 24
 Le Fèvre O. et al., 2015, *A&A*, 576, A79
 Le Fèvre O. et al., 2005, *A&A*, 439, 845
 Leistedt B., Mortlock D. J., Peiris H. V., 2016, *Mon. Not. Roy. Astron. Soc.*, 460, 4258
 Lilly S. J. et al., 2007, *ApJS*, 172, 70
 Lima M., Cunha C. E., Oyaizu H., Frieman J., Lin H., Sheldon E. S., 2008, *Mon. Not. Roy. Astron. Soc.*, 390, 118
 Loh E. D., Spillar E. J., 1986, *ApJ*, 303, 154
 LSST Science Collaboration et al., 2009, *arXiv:0912.0201*
 Martí P., Miquel R., Castander F. J., Gaztañaga E., Erikssen M., Sánchez C., 2014, *Mon. Not. Roy. Astron. Soc.*, 442, 92
 Masters D. et al., 2015, *ApJ*, 813, 53

- Melchior P. et al., 2016, arXiv:1610.06890
- Ménard B., Scranton R., Schmidt S., Morrison C., Jeong D., Budavari T., Rahman M., 2013, arXiv:1303.4722
- Miller L. et al., 2013, *Mon. Not. Roy. Astron. Soc.*, 429, 2858
- Moles M. et al., 2008, *AJ*, 136, 1325
- Molino A. et al., 2013, arXiv:1306.4968
- Morrison C. B., Hildebrandt H., Schmidt S. J., Baldry I. K., Bilicki M., Choi A., Erben T., Schneider P., 2016, arXiv:1609.09085
- Newman J. A., 2008, *ApJ*, 684, 88
- Newman J. A. et al., 2015, *Astroparticle Physics*, 63, 81
- Newman J. A. et al., 2013, *ApJS*, 208, 5
- Rau M. M., Seitz S., Brimiouille F., Frank E., Friedrich O., Gruen D., Hoyle B., 2015, *Mon. Not. Roy. Astron. Soc.*, 452, 3710
- Sadeh I., Abdalla F. B., Lahav O., 2016, *PASP*, 128, 104502
- Samuroff S., Troxel M. A., Bridle S. L., Zuntz J., MacCrann N., Krause E., Eifler T., Kirk D., 2017, *Mon. Not. Roy. Astron. Soc.*, 465, L20
- Schmidt S. J., Ménard B., Scranton R., Morrison C., McBride C. K., 2013, *Mon. Not. Roy. Astron. Soc.*, 431, 3307
- Schneider M., Knox L., Zhan H., Connolly A., 2006, *ApJ*, 651, 14
- Sheldon E. S. et al., 2004, *AJ*, 127, 2544
- Spinelli P. F., Seitz S., Lerchster M., Brimiouille F., Finoguenov A., 2012, *Mon. Not. Roy. Astron. Soc.*, 420, 1384
- Tasca L. A. M. et al., 2016, arXiv:1602.01842
- Umetsu K., Broadhurst T., Zitrin A., Medezinski E., Coe D., Postman M., 2011, *ApJ*, 738, 41
- von der Linden A. et al., 2014, *Mon. Not. Roy. Astron. Soc.*, 439, 2
- Xiao Y., Gordon A., Yakovlev A., 2006, *Journal of Statistical Software*, 17, 1